Preparation of Ag releasing biomedical contrivance using ZnO–reduced graphene oxide hybrid

1Rajeswari Rakkappan, 2Kavitha Alagappan, 3Ananda Babu Sairam
1Research Scholar, 2Assistant Professor, 3Assistant Professor
1Alagappa University,
2Sree Sevugan Annamalai College,
3Sri Venkateswara College of Engineering

Abstract - **One pot-hydrothermal method is employed for synthesis of distinctive morphology Ag-RGO/ZnO hybrid materials, without using any chemical reductants. It shows potential applications to explore their biomedical associated activity to help. The synthesized hybrid was characterized by subsequent techniques. The X-ray diffraction (XRD) and X-ray photo electron spectroscopic (XPS) analysis confirmed the successful decking of Ag on the RGO-ZnO sheets. Fourier transform infrared spectroscopy (FT-IR), inveterate the presence of functional groups. Scanning electron microscopic (SEM) observations showed that the prepared composite displayed a uniform morphology. The SAED patterns of the Transmission electron microscopic studies (TEM), revealed that the prepared Ag-RGO/ZnO hybrid has the size of 23 nm. The experimental results have revealed that the prepared hybrids exhibited significantly excellent performance towards gram negative bacterial and fungal pathogens, simultaneously its antioxidant capacity and cytotoxicity nature is determined by various methods the results revealed that, dose dependent activity was observed on Human embryonic kidney 293 cells. This Ag releasing eminence may take the form of devices, implants, machines, medicines and technologies. Make inquiries also applies their understanding of DNA to numerous real-world applications.**

keywords - **Ag-RGO/ZnO, Hybrid, anticancer, Ag release**

I. Introduction (Heading 1)

Reduced graphene oxide (RGO) blend with Ag and Au nanoparticle using chitosan as both a reducing and a stabilizing agent that exhibit good electrochemical activity [1]. The ternary composite composed of RGO, Cu2O and Cu quantum dot as efficient and lightweight microwave absorbing material was synthesized at room temperature by using NaBH4 [2]. Composites with obviously enhanced microwave absorption properties were successfully fabricated by a rational one-pot simplified co-precipitation route, which avoided the usage of an inert gas and any additional chemical agents. The strategy described as a simple and large-scale route to yield RGO–Fe3O4 composites would find wide applications in the microwave absorbing area [3]. A magnetically separable Fe3O4@CuO-RGO core-shell hetero structured photocatalysts were synthesized. The decoration of Fe3O4@CuO spheres on both sides of graphene sheets as well as the reduction of graphene oxide. The as-prepared Fe3O4@CuO-RGO composites possessed enlarged visible light adsorption range and enhanced charge separation efficiency compared with that of the pure CuO and Fe3O4@CuO. Also, the unique structure afforded Fe3O4@CuO-RGO desirable photocatalytic activity and stability for the degradation of methylene blue under visible-light irradiation [4]. PANI nanoparticles were successfully anchored on the surface of RGO sheets by using RGO–MnO2 hybrids as both of the templates and oxidants for aniline monomer during the process of polymerization. The RGO–PANI hybrid device exhibited much better (3.4 and 10.4 times, respectively, with the concentration of NH3 gas at 50 ppm) response to NH3 gas than those of the bare PANI nanofiber sensor and bare graphene device. The combination of the RGO sheets and PANI nanoparticles facilitated the enhancement of the sensing properties of the final hybrids, and pave a new avenue for the application of RGO–PANI hybrids in the gas sensing field [5]. The RGO sheets wrapped ZnO nanoparticles and nanorods very tightly. After the emission of photo electrons from ZnO, RGO in ZnO–RGO can effectively transfer the photo electrons to exhibit a high performance and reproducibility in photocatalytic degradation toward methylene blue (MB) absorbed on the surface of RGO through π–π conjugation. The ZnO–RGO can hinder the recombination of photo electrons and holes to enhance the photocatalytic degradation of methylene blue [6]. The enhanced performance can be explained by the modification of the electronic structure of Pd by Ni after alloy formation and the large specific surface area and excellent electron conductivity of the rGO support [7]. TiO2–Fe3O4/RGO composites with good magnetism and photocatalytic activity were prepared by a facile hydrothermal method with RGO and magnetic TiO2 as starting materials in ethanol–water solvent. The photocatalytic degradation of MB by TiO2–Fe3O4/RGO composites under visible light irradiation was examined by varying the operational parameters such as catalyst amount, irradiation time, pH and initial MB concentration [8]. Hybrid nanocomposites of reduced graphene oxide/multi-walled carbon nanotubes/zinc ferrite (RGO/MWCNTs/ZnFe2O4) were fabricated by a facile one-pot hydrothermal strategy. The obtained hybrid nanocomposites were potential candidates for application in the field of microwave absorption [9]. Au-reduced graphene oxide/PDDA nanocomposites (Au-RGO/PDDA) can be rapidly synthesized through a facile, cost-effective, one-pot method with the use of poly(diallydimethylammonium chloride) (PDDA) as both reducing and stabilizing

agents. Au-RGO/PDDA sensor was also demonstrated for the determination of nitrite ion in lake water, meat and dairy products samples with acceptable results [10]. Hummers' method (KMnO4, NaNO3, H2SO4) is the most common method used for preparing GO. Excluding NaNO3 and optimizing the acids ratios of H2SO4/H3PO4 in order to improve the efficiency of the oxidation process as a green, effective, and low-cost deoxygenation agent for mass production of RGO [11]. Porous RGO-wrapped magnetite nanoparticles were obtained by a simple precipitation reaction followed by freeze drying and heating at 80 °C in air. These composites exhibit very good lithium cycling properties and minimal capacity fading. [12]. Electronic gas sensors and super capacitors have been fabricated with the caffeic acid -RGO and show good performance, which demonstrates the potential of caffeic acid -RGO for sensing and energy storage applications [13]. The graphene shell could effectively protect the internal CdS microsheres from photocorrosion, and the composite showed an excellent recyclability property for its photocatalytic applications [14]. Synergistic heteroconjunctions in TiO2/RGO facilitating a fast electron transfer at the interface among them. This synergistic approach could prove useful for the design and development of other visible light active photocatalysts with high chemical stability [15]. The cubic Cu2O-RGO nanocomposites demonstrate enhanced visible-light-driven photocatalytic activity for methyl orange dye with a 100% degradation rate in 100 min. The enhanced photocatalytic performance is mainly attributed to the increased charge transportation, effective separation of photoelectrons from vacancies, and the improved contact area [16]. Polyethersulfone based mixed matrix nanofiltration membrane was developed by blending with partially reduced graphene oxide (rGO)/TiO2 nanocomposite. The membranes showed better dye removal performance than the bare Polyethersulfone [17]. There are lesser studies on fabrication of Ag decking RGO/ZnO hybrid. However, in majority reports the effect of the amount of ZnO in RGO matrix upon performance of instance Ag releasing is explored. Therefore, in this study, RGO/ZnO hybrid is incorporated as anti cancer agent and the effect of Ag concentration in against Human embryonic kidney 293 cells (HEK 293) cell line is investigated.

II. MATERIALS AND METHODS

The chemicals and reagents such as graphite flakes, sulfuric acid (H2SO4), hydrogen peroxide (H2O2 -30%), potassium permanganate (KMnO4), zinc nitrate hexahydrate (ZnNO3)2.6H2O), sodium nitrate (NaNO3), silver nitrate (AgNo3), hydrochloric acid (HCl 37%) used as source material for synthesis of nanocomposite were purchased from Sigma-Aldrich and consumed without purification. Graphite flakes was used to prepare Graphene oxide by modified Hummer's method [18-19] 1 g of graphite powder was mixed with cold H2SO4 (23mL) then NaNO3 (2.5g) was added to the mixture and stirred it in an ice bath for half-an-hour, 9g of Kmno4 was added vigorously with continuous stirring. The temperature of the mixture was maintained by 20 °C and prevented not to exceed the temperature. The content of the mixture was stirred continuously for 4 h. Temperature is shooted to 95°C while deionized water was added. The experimental procedure was maintained for 12 h. 3mL of 30% H2O2 and 140 mL of D.I water is added to terminate the yellow coloured suspension. The solution was washed with 2mL of 1:1 HCl and water for more times, finally the precipitate was centrifuged and dried in an oven over night for 60°C

Nanocomposite was prepared by the following procedure, 0.1mg/mL of Graphene oxide (GO) dispersion was sonicated for 1h. Then (50mM) of Zinc nitrate hexahydrate and silver nitrate solution was added into the GO dispersion by continuous stirring for 1h. All the above mentioned contents were stirred vigorously for 0.5h; blackish gray slurry was obtained, it was then transferred into 50mL Teflon-lined autoclave and heated to 140°C for 4 h. After completion of the reaction the liquid in the superannuated phase was discarded and the precipitate was washed with water, dried in an oven at 60 °C it is labeled as Ag-RGO-ZnO nanocomposite. The synthesized sample's crystal phase information of was characterized using an X-ray powder diffractometer (XRD). The (X'Pert PRO PAN Analytical diffractometer) of Cu Kα radiation (kα-50.15406 nm) with the scanning rate of 0.01°/step. Fourier transform-infrared (FT-IR) spectra RXI [Perkin Elmer] in the range of 4000–400 cm−1was employed to analyze the functional groups of the prepared nanocomposite at room temperature. Scanning electron microscope (SEM) was used to elucidate the morphology of the composite SEM images of the samples were depicted using Quanta FEG-250; HR-SEM. Transmission electron microscope (TEM) image of the synthesized nanocomposite was obtained on a (PHILIPS CM 200) at an acceleration voltage of 200 kV. The sample was dispersed in ethanol solution and then transferred onto Cu/lacey carbon TEM grids. The X-ray photoelectron spectroscopy was examined by (XPS, PHI 5300)

The antibacterial activities of the synthesized Ag-RGO–ZnO nanocomposites were examined by an agar well diffusion method against four bacterial pathogens Pseudomonas aerunginosa, Klebsiella pneumonia, (gram-negative) Bacillus thuringiensis, Bacillus cereus, (gram-positve) and two fungal pathogens such as Candida albicans, Candida trophicans, with standard antibiotics amikacin and ketoconazole recommended by clinical and laboratory standard Institute 2006 in Muller Hinton agar (MHA SRL chemical) medium. The cultures were swabbed on the petri plates; about 3 mm diameter of agar wells was punched out of the plates. Ag-RGO–ZnO nanocomposite was loaded in each well. Dimethyl sulfoxide (DMSO) chemical was served as negative control and the strains were grown in nutrient broth. Under the optimum conditions, the plates were incubated at 38°C for 24 h. The diameter of the inhibition zone was measured and expressed in millimeter, optical images of the plates were taken, the composite showing maximum antimicrobial activity for each pathogen was noted and tabulated.

Antioxidant activities of the synthesized sample were examined by several in vitro test procedures Single activity test model should not be concluded. For evaluating the best model, different in vitro methods were performed and discussed [20]. The basic radical scavenging activity of Ag-RGO–ZnO composite was examined against various antioxidants assays like hydroxyl radical, peroxides, and the model stable radical 2, 2-diphenyl-1-picrylhydrazyl (DPPH). Among all scavenging methods, DPPH is rapid inexpensive and simple. The scavenging sites are associated with the pristine graph. Three replicates were made to test each sample.

Natural DPPH free radical scavenging activity was determined by Molyneux method [21] (50–200 µg/mL) concentrations of composite were added, at an equal volume of a methanolic solution of DPPH. The mixture was reacted at room temperature in the dark for 30 min. Ascorbic acid was used as a standard control. After 30 min the optical density of DPPH radical is

monitored, the absorbance (A) was measured at 518 nm and converted into the percentage antioxidant activity using the equation:

$$\% = [(A_{(0)} - A)/A_{(0)}] = 100$$

Where;

Ao was the absorbance of the control and

A1was the absorbance in the presence of composite

The Nitric oxide (NO) scavenging activity was determined by the method [22]. Sodium nitroprusside of 100 µL was incubated with 100 µL composite at different concentrations for 60 min, at room temperature under the light. All solutions were prepared in phosphate buffer. After incubation, The generated NO radical reacted with oxygen and produce nitrite ions, (NO)which were treated with 100 µL of Griess reagent and incubated mixture The mixture was incubated at room temperature for 10 min and the absorbance of the chromophore formed during the diazotization of nitrite with sulphanilamide and subsequent coupling with naphthylehylendiamine was read at 562 nm. Percent inhibition was determined by where A control = Absorbance of control reaction and A test = Absorbance in the presence of the sample of test compounds. 3-[4,5-dimethylthiazol-2-yl]2,5-diphenyltetrazolium bromide (MTT) is a yellow water-soluble tetrazolium salt. Amitochondrial enzyme in living cells, succinate-dehydrogenase, cleaves the tetrazolium ring, converting the MTT to an insoluble purple formazan. Therefore, the amount of formazan produced is directly proportional to the number of viable cells. After 48 h of incubation, 15 µL of MTT (5 mg/mL) in phosphate buffered saline (PBS) was added to each well and incubated at 37 °C for 4 h. The medium with MTT was then flicked off and the formed formazan crystals were solubilized in 100 µL of DMSO and then measured the absorbance at 490 nm using micro plate reader. The absorbance of the test sample was normalized by subtracting with absorbance of respective concentration of blank and the percentage cell viability was then calculated with respect to control as follows

$$\% \text{ Cell viability} = ([A]\text{Test})/([A]\text{control} \times 100)$$

In-vivo Experiment

Female (Albino White) mice of 6–8 weeks of age were procured from the Venture Institute of Biotechnology (VIBR). The protocol was approved by the Animal Ethics Committee of VIBR, Madurai. All experiments on animals were performed as per the guidelines of the Committee for the Purpose of Supervision of Experiments on Animals (CPCSEA), national regulatory body for experiments on animals. In all animal experiments, mice were divided into 3 groups, each group consisting of 6 mice unless mentioned otherwise.

The prepared composite was induced paw edema in mice is a well established model of acute inflammation for screening of anti-inflammatory agents. Anti inflammatory activity of compound was studied using paw edema in mice model as per previously described method. Briefly, inflammation was induced in right hind paw of mice by subcutaneous injection of 0.5 ml of 1% composite. The mice were pretreated with intra-peritoneal injection of standard drug, Paracetamol (100 mg/kg) and the drug, subcutaneously (8 mg/mouse) one hour before administration of compound. Edema in the paw was measured at hourly interval starting from zero hour up to 4 hours and compared with the controls. The inhibitory effect was determined by using following formula: % Inhibition= (Initial –Final X 100)/Initial

III. RESULTS AND DISCUSSIONS

Figure.1 (a-c) shows XRD patterns of RGO, RGO-ZnO and Ag decked RGO-ZnO hybrid; (a) shows broad diffraction peak at 24.42° that is attributed to (002) plane of RGO [23]. The strong four diffraction peaks at 36.32°, 47.63°, 62.80° and 76.02° are attributed to the (101), (102), (103) and (202) crystalline planes of ZnO respectively; five minor peaks at 31.4º, 34.4º, 56.6º, 62.8º and 68.5º corresponds to the (100), (002), (110), (103) and (112) planes of ZnO respectively (Figure. 1 b). All peaks are matched with the JCPDS card no: 36-1451. The diffraction peaks possess single phase wurtzite structure of ZnO [24] Ag decked RGO-ZnO hybrid exhibits strong four diffraction peaks at 38.12°, 44.27°, 64.52° and 77.5°, which are attributed to the (111), (200), (220) and (311) crystallographic planes of face-centered cubic of Ag respectively (Figure. 1.c) that are good agreement with JCPDS data (JCPDS No. 04-0783) [25].

After doping of Ag, the peak intensities of RGO and ZnO are diminished due to the presence of a small quantity of RGO and distribution of Ag NPs onto the RGO-ZnO surface [26]. The average particle size of Ag decorated RGO-ZnO hybrid can be calculated from the width of lines in the XRD spectrum with the help of Scherrer's equation. The average grain size is found to be 24 nm and also particle size distribution is concurrence with TEM. From the XRD result, it is confirmed that the formation of Ag decked RGO-ZnO hybrid Figure.2. (a-d) depicts the HR-TEM images of RGO, ZnO NPs, RGO-ZnO hybrid and Ag decked RGO-ZnO hybrids. RGO shows wrinkled and lamellar structures with a transparent sheet Figure.2. (a) [27]. ZnO NPs exhibited (b) rod-like morphology that is polycrystalline in nature with wurtzite structure, but this ZnO NPs are randomly distributed on the RGO sheets that are sandwiched between RGO sheets (c) [28]. In Ag decked RGO-ZnO hybrid, a good number of smaller spherical Ag NPs and big spherical ZnO NPs are noticed. The Ag NPs are uniformly scattered, but ZnO NPs are randomly distributed on the graphene sheets. The rod morphology is not observed over the RGO sheets because of strong electrostatic and electron transfer interactions between ZnO NPs and RGO sheets [29].

The average Ag-RGO-ZnO hybrid fleck size of is found to be below 25 nm. The crystallographic structure of the Ag decked RGO-ZnO hybrid was characterized by SAED. As observed from Figure.2d, the RGO-ZnO shows a typical RGO lattice fringe, and the distinct diffraction spots of Ag is also shown on the SAED pattern in Figure.2d. The diffraction profile generated by Ag decked RGO-ZnO hybrid structure. HR-SEM with EDX analysis of synthesized Ag decking RGO-ZnO hybrid is illustrated in Figure.3.(a-c). In Ag-RGO-ZnO hybrid, the RGO exhibited thin sheets like structure, randomly aggregated with distinct edges, wrinkled surfaces and folding [30]. The mean sheets dimension is noticed at 3µm. ZnO NPs shows spherical like structure with faceted growth uniformly distributed and the size of the particle is below 25 nm [31].

The ZnO NPs are well anchored on the RGO and some of the particles are intercalated between the graphene sheets to form sandwich structure; many small white spherical dot like Ag NPs are randomly distributed on the surface of the RGO sheet. After Ag NPs decorated with RGO-ZnO, the rod morphology of ZnO is fully distorted to spherical [32]. The average particle size of the Ag decked RGO-ZnO hybrid is found to 24 nm. The EDX spectrum Figure.3 (d) clearly shows the existence of elements such as Ag, Zn, C, O and S in the RGO, ZnO and its hybrids. The FT-IR spectra of RGO, RGO-ZnO, and Ag-RGO-ZnO hybrid are shown in Figure. 4 (a-c). The peaks (a) noticed at 3430 cm-1, 1641cm-1 and 1050 cm-1 are related to the OH, C=O and C-O groups respectively, indicating the graphite structure. Similar peaks (b) are also obtained in RGO-ZnO hybrid, but the peak intensity is decreased than RGO. In addition, the peak observed at 486 cm-1 indicates the hexagonal ZnO [33]. For Ag decked RGO-ZnO hybrid, all the similar functional groups are present and one additional peak at 450 cm-1 is observed indicating the presence of Ag and ZnO NPs. The peaks (OH, C=O and C-O) intensities are decreased and slightly shifted to lower side. This trend is shows confirmation of forming Ag particles decking on the surface of RGO-ZnO through a chemical bond or simple electrostatic attraction [34]. This kind of Ag decking is may facilitate to open new technique of biological applications on RGO. The XPS spectral analysis provides information about the surface structure, chemical interaction and oxidation states of ions. Figure.5. (a-e) shows XPS spectra of Ag decked RGO-ZnO hybrid survey spectrum, Ag 3d peak, Zn 2p peak, O 1s peak and C 1s peak; (a) reveals the presence of Ag, Zn, O, and C elements; in Ag 3d peak spectrum, two main peaks observed at 368 eV and 375 eV corresponding to Ag 3d5/2 and Ag 3d3/2 respectively (b) [35]. Two peaks observed for Zn 2p core level at 1024.2eV and 1046.4 eV coincides with the Zn 2p1/2 and Zn 2p3/2 respectively, it confirms the oxidation state of Zn as Zn2+ (c) [36]. The O 1s peak centered at 531.2 eV and 535.7 eV is attributed to the oxygen absorbed from water and oxygen attached to the RGO as C-O bond (d). The C1s spectrum showed three peaks at 284.6 eV, 286.4 eV and 287.6 eV, which are related to the C-C bond of graphite carbon, C-O and C=O respectively. The C-C bond is sharp with intense peak and C-O bond is broadened peak due to the loss of oxygen during the reduction of GO into RGO (e). The XPS result confirms that the RGO base is poised of elements in the state of Zn2+, Ag (0). It helps to confirming formation of Ag decked RGO-ZnO hybrid. The synthesized hybrid material (Ag-RGO-ZnO) was examined for Antimicrobial, Antioxidant and Cytotoxicity behavior. The antibacterial activity of RGO, RGO-ZnO hybrid, and Ag decked RGO-ZnO hybrid was evaluated against gram-negative (Klebsiella pneumonia, Pseudomonas aerunginosa) and gram-positive (Bacillus cereus and Bacillus thuringiensis) bacterial strains by agar well disc diffusion method. The zone of inhibition of all the synthesized material is measured by the diameter and the results towards the selected bacterial strains are represented in Figure.6 (a-l). It is found that Ag decked RGO-ZnO hybrid exhibited superior antibacterial activity against gram-negative bacterial strains compared to RGO-ZnO hybrid, and RGO [37]. This improved activity may be due to the formation of reactive oxygen species (OH°, O2- and H2O2) which may react with electron-donating groups of thiol, carboxylates, hydroxyl, and amides on the proteins present on the bacterial surface thereby creating cavities on the cell wall [38]. RGO has a high surface area that improves the adsorption of water and oxygen molecules and reacts with electrons to bring up excess reactive oxygen species. The Ag particles decked out and interact with bacteria allowing a strong contact between Ag edge surface and bacteria to create cavities on the cell wall that increases the cell permeability and eventually leads to bacterial death [39]. Also, the presence of Ag and ZnO in hybrid may be attached to the surface of the cell membrane and easily interact with sulphur and phosphorous-containing DNA [40-43]

Importantly, Gram-negative bacteria have shown a higher zone of inhibition than Gram-positive bacteria, this is because of the smaller spherical particle size of Ag decorated on the hybrid easily penetrates inside the bacterial membrane and showed improved antibacterial activity. The effect of the antifungal activity of Ag decked RGO-ZnO hybrid and Ag discharge against Candida albicans and Candida tropicalis is shown in Figure. 6. (i-l) The result indicated that RGO and its composite shows antifungal activity owing to the direct contact with the cell walls of fungi. As expected the combination of metal (Ag) and metal oxide (ZnO) decked on the RGO surface area (Ag-RGO-ZnO) hybrid has shown effective antifungal activity than bare Ag. The composite interacts with organic functional groups of chitin and other polysaccharides on the cell walls of fungi. The reason is slow release of Ag+ ions from the hybrid, this Ag NPs can enter the cell wall and kill the fungi through several processes including breaking the cell wall membrane, destroy the structure of proteins, and interrupting the DNA synthesis. Moreover, the small sizes of Ag NPs have good chance to interact with cell membrane over the larger surface area. The synthesized hybrid (Ag-RGO-ZnO) has shown good quality antimicrobial properties towards gram-negative and fungal pathogens. Figure. 7 shows the histogram representation of Ag-RGO-ZnO hybrid and bare Ag against standard bacterial strain- amikacin and fungal pathogen-ketoconazole. DPPH (2-diphenyl-1- picrylhydrazyl) molecules contain stable free radical which has been used to evaluate the radical scavenging ability of antioxidants. Figure.8 shows antioxidant activity of RGO, RGO-ZnO and Ag decorated RGO-ZnO hybrid measured in terms of their DPPH free-radical-scavenging activity compared with standard antioxidant-ascorbic acid. The result revealed that Ag decorated with RGO-ZnO hybrid has effectively reduced DPPH radical, when compared to RGO-ZnO, Ag, ZnO and RGO. When the concentration of hybrids increased, the DPPH radical scavenging antioxidant activity is also increased. The improved activity may be due to reducing capacity, prevention of chain initiation, and radical scavenging [44-46]. In addition, the improved antioxidant property is due to the presence of small spherical Ag NPs present in the hybrid. It is assumed that, the combined effect of metal (Ag) and metal oxide ZnO on RGO sheets have shown 66% antioxidant activity at 200 µg/mL. Nitric oxide (NO) is a free radical because it possess unpaired electron and displays a reaction between proteins and other free radicals. It reacts with superoxide radical, and forms a reactive peroxynitrite anion (ONOO-) [47]. Therefore, RGO, RGO-ZnO and Ag-RGO-ZnO at different concentrations were assessed for their nitric oxide free radical scavenging activity by in vitro method. Diazotization takes place between the nitrite ions and sulphanilamide acid and coupled with naphthyl ethylenediamine. The formation of pink color was measured at 548 nm [48]. It has predicted that all the prepared components scavenged nitrite radical in a dose dependent manner. The nitric oxide scavenging activity of RGO, ZnO, Ag, RGO-ZnO and Ag decorated RGO-ZnO hybrid is presented in Figure.9. The results revealed that the antioxidant activity of Ag-RGO-ZnO hybrid has exerted 74.1% at 200 µg/mL. The result proposed that Ag-RGO-ZnO hybrid showed better activity than RGO, ZnO, Ag, RGO-ZnO hybrids. Synthetic antioxidants are an alternative source for oxidative stress. A

great number of graphene based metal oxide have been recognized as antioxidants. Based on the results, it is proved that Ag-RGO-ZnO hybrid is a potent antioxidant. When comparing the synthesized materials RGO, ZnO, Ag, RGO-ZnO and Ag-ZnO-RGO with standard ascorbic acid, the antioxidant potency is in the order of RGO < ZnO< RGO-ZnO < Ag< Ag-RGO-ZnO. Finally it is proven that Ag-ZnO-RGO is the most potent nitric oxide radical scavenger than that of other composites. These results revealed that the scavenging activity of the hybrid exerted 74.1% at 200 µg/mL in nitric oxide method, whereas 66% radical scavenging activity is observed in DPPH method. Biocompatibility of the synthesized material was examined, initially its toxicity should be performed on biological cells. The application of the RGO, RGO-ZnO, and Ag-RGO-ZnO hybrids in biomedical field has been examined in human embryonic kidney cell line HEK 293. The optical microscopic images of the results obtained are displayed in Figure.10. (a-e) and the graphical representation of the cell viability of hybrid is shown in Figure.11 [49]. The biocompatibility of RGO coupled with Ag and ZnO shows improved cell viability [50]. At lower concentration (6.5 µg/mL), 98% of cells were found to be alive. The entry of Ag NPs inside the cell, deactivates the enzymes, breaks the hydrogen bonds of DNA and denatures its [51].

Hearsay revealed that Ag NPs interfere with electron transfer chain [52] causes ATP leaking [53] and produce free radicals [54]. Small size of the nanoparticles possesses strong cell viability [55-56]. The small, spherical size of the hybrid has an effect to penetrate it into biological membranes and initiated immunological reactions [57]. Electrostatic attraction between the hybrid and the cell plays an important role in increased cytotoxicity [58]. At higher concentrations (25 µg/mL), cell viability decreases; the rounded cell morphology at few places in Figure.10 d&e are the evident for the toxic behavior of the hybrid. The toxicity is highly concentration dependent. Synthesized hybrid possesses good cell viability and chemical stability at 6.5µg/mL; this is due to the decoration of small, spherical Ag NPs on RGO-ZnO matrix. IC50 values are lesser than that of RGO and ZnO nanoparticles. It is evident that modification on structural morphology and selection of non-toxic incorporation materials will increase the biocompatibility of the synthesized hybrid. Anti-Inflammatory activity of Ag-RGO-ZnO composite in mice model was analyzed with induced paw edema in mice. In our studies, subcutaneous injection of composite caused an increase in paw size in mice due to edema, thus indicating acute inflammation of paw. The thickness of paws in different groups of mice following treatment with control, standard and compound. The results were revealed in Table:1. Ag-RGO-ZnO composite was subjected for their anti-inflammatory activity using formalin induced paw edema method. The results for the percentage of inhibition of paw edema were depicted in Table1. The relative percentage of edema induced inhibition by the test composite Ag-RGO-ZnO was recorded after 1, 2, 3 and 4 causing edema hours with 6.55%, 22.12%, 30.5% and 52.12% respectively. Then the percentage inhibition was progressively increased and reached a maximum inhibition with 52.12% at 4 hours. While the reference standard (Paracetamol) revealed a less percentage of inhibition edema with 31.56% after four hours compared to the test compound Ag-RGO-ZnO.

IV. Conclusion

The hybrid (Ag-RGO-ZnO) was prepared by one-pot hydrothermal simple method at low temperature. The crystalline structure was confirmed by XRD analysis The hybrid exhibited four diffraction peaks at 38.12°, 44.27°, 64.52°, and 77.5° attributed to the (111), (200), (220) and (311) crystallographic planes of face-centered cubic of Ag respectively. The functional groups present in the hybrid were confirmed by FT-IR analysis. SEM images have shown; spherical ZnO and spherical dot like Ag NPs fully scattered on the RGO sheets, TEM analysis confirmed the presence of 20-30 nm size of the Ag, ZnO NPs. XPS has shown the elemental composition of the prepared hybrid. Ag-decorated RGO-ZnO sheets have shown remarkable improvement in antimicrobial properties. Agar well diffusion method was employed for the estimation of MIC values to evaluate the antimicrobial activity of the composite. Results showed that the MIC value of gram-negative bacteria (Klebsiella pneumonia, Pseudomonas aureginosa) was found to be 17 µg/mL, 15 µg/mL compared with the standard (amikacin). This efficacy of the hybrid may be owing to the structural difference in the cell wall composition of the gram-positive and gram-negative bacteria. It is revealed that the synergistic effect from both RGO-ZnO and Ag have resulted in the efficacy. The hybrid exhibited strong antioxidant potential in Nitric oxide scavenging method 74.1% was observed against the standard. The synthesized hybrid is further examined for its cell viability against human embryonic kidney cell (HEK 293), at a minimum concentration (6.5 µg/mL) the maximum (98%) cell viability is observed. Thus the synthesized hybrid (Ag-RGO-ZnO) may be a potential candidate and good source for Ag delivery applications.

References

[1] Guoa Y, Suna X, Liua Y, Wang W, Gao H Q.J. One pot preparation of reduced graphene oxide (RGO) or Au (Ag) nanoparticle-RGO hybrids using chitosan as a reducing and stabilizing agent and their use in methanol electrooxidation. Carbon. 2012:50:2513-23.

[2] Zong M, Huang Y. Haiwei, Yang W, Panbo Z, Wang L.L. Facile preparation of RGO/Cu2O/Cu composite and its excellent microwave absorption properties. Mater Lett. 2013;109:112-15.

[3] Zong M. Huang Y, Zhao Y, Sun X, Didi Luo C.Q, Zheng J. Facile preparation, high microwave absorption and microwave absorbing mechanism of RGO–Fe3O4 composites. RSC Adv. 2013;3:23638-48.

[4] Lizhong J.D, Jinjuan L, Zhengwei X, He Z.G, Chen H. Low-temperature preparation of magnetically separable Fe3O4@CuO-RGO core-shell heterojunctions for high-performance removal of organic dye under visible light. J. Alloys Compd. 2016;688:649-56.

[5] Huang X, Hu N, Gao R, Yu Y, Wang Y, Yang Z, Kong E.S.W, Wei H, Zhang Y. Reduced graphene oxide–polyaniline hybrid: Preparation, characterization and its applications for ammonia gas sensing. J.Mater.Chem. 2012;22:22488-95.

[6] Zhou X, Shi T, Zhou H, Hydrothermal preparation of ZnO-reduced graphene oxide hybrid with high performance in photocatalytic degradation. App Surf Sci. 2012;258:6204-11.

[7] Yiyi S, Zhouguang L, Wenguang F, Simon J, Michael K.H. Facile preparation of PdNi/rGO and its electrocatalytic performance towards formic acid oxidation. J. of Mat. Chem. A.2014;11:3894-98.

[8]. QiLi Z, Wang HL, YunZi L, Jun J, Shan Y, Preparation and photocatalytic performance of magnetic TiO2-Fe3O4/graphene (RGO) composites under VIS-light irradiation.Ceram. Int.2015;41:10643.
[9] Shu R, Weijie, LiXian, Zhou, Dongdong, Gengyuan T, Ying Z, GanJianjun, ShiJieHe. Facile preparation and microwave absorption properties of RGO/MWCNTs/ZnFe2O4 hybrid nanocomposites. J. Alloys Compd.2018;743:163-74.
[10] Feng S, Jing J, Lun Wang J. One-pot preparation of Au-RGO/PDDA nanocomposites and their application for nitrite sensing.Sens. Actuators B Chem.2015;208:36-42.
[11]. Fathy M, Goma A, Taher FA, Magda El-Fass M, Hady AE, Kashyout B. Optimizing the preparation parameters of GO and rGO for large-scale production.J. Mater.Sci.2016;51:5664–75.
[12] Hameed A.S, Reddy M.V, Chowdari B.V.R, Vittal JJ. Preparation of rGO-wrapped magnetite nanocomposites and their energy storage properties.RSC Adv.2014;4:64142-50.
[13] Bo Z, Shuai X, Mao S, Yang H, Qian J, Chen J. Yan J, Kefa Cen. Green preparation of reduced graphene oxide for sensing and energy storage applications. Scientific Reports2015;4:4684.
[14] Liu H, Lv T, Xiaohua W, Chunkui, Zhenfeng Z. Preparation and enhanced photocatalytic activity of CdS@RGO core–shell struct ural microspheres.App.Surf.Sci.2014;305:242–46.
[15] Huanga M, Jianhua, Qun Y, Wenli H, Minguang S, BinLia F, Tang L, Metalorganicframeworkg-C3N4/MIL-3(Fe)heterojunctions withenhanced photo catalytic activity for Cr(VI) reduction under visiblelight. Appl. Surf. Sci.2017;425:107–16.
[16] Zhang W, Li X, Yang Z, Tang X, Ma Y, Li M, Hu N, Wei H, Zhang Y, In situ preparation of cubic Cu2O-RGO nanocomposites for enhanced visible-light degradati on of methyl orange. Nanotech.2016;27:26.
[17] Safarpoura M, Vatanpour V, Khataee A. Preparation of a Novel Polyvinylidene Fluoride (PVDF) Ultrafiltration Membrane Modified with Reduced Graphene Oxide/Titanium Dioxide (TiO2) Nanocomposite with Enhanced Hydrophilicity and Antifouling Properties. Desalination. 2016;393:65.
[18] Hummers WS, Offeman RE. Preparation of Graphene oxide. J. Am. Chem. Soc.1958;80:1339.
[19] Karthikeyan K, Mohan R, Kim S.J. Graphene oxide as a photocatalytic material.Appl. Phys. Lett.2011;98:244101.
[20] Badarinath AV, Rao KM, Chetty CMS, Ramkanth V, Rajan TVS, Gnanaprakash K, A Review onIn-vitro Antioxidant Methods:Comparisions. Correlations and Considerations, Int. J.PharmTech Res.2010;2:1276-85.
[21] Menaga D, Rajakumar S,. Ayyasamy PM. Free radical scavenging activity of methanolic extract of pleurotus florida mushroom. Int. J. Pharm. Pharm. Sci.2015;5:975.
[22] Sousa C, Valentao P,. Ferreres FR, Seabra M, Andrade PB, Tronchuda Cabbage (Brassica oleracea L. var. co stata DC): Scavenger of Reactive Nitrogen Species. J. Agric. Food. Chem.2008;56:4205–11
[23] Nethravathi C. Rajamathi M. Chemically modified graphene sheets produced by the solvothermal reduction of colloidal dispersions of graphite oxide. Carbon.2008;46:1994-98.
[24] Fu D, Han G, Chang Y, Dong J. The synthesis and properties of ZnO–graphene nanohybrid for photodegradation of organic pollutant in water. Mater. Chem. Phys.2012;132:673–81.
[25] Bera S, Ghosh M, Pal M, Das N, Saha S, Dutta SK, Jana S. Synthesis, characterization and cytotoxicity of europium incorporated ZnO–gra phene nanocomposites on human MCF7 breast cancer cells.RSC Advances.2014;4:37479-90.
[26] Kaschner A, Haboeck U, Strassburg M, Strassburg M, Kaczmarczyk G, Hoffmann A, Thomsen C,.Zeuner A, Alves HR, Hofmann DM, Meyer BK. Nitrogen-related local vibrational modes in ZnO:N. Appl. Phys. Lett.2002;80:1909.
[27] Bera S, Khan H, Biswas I, Jana S. Polyaniline hybridized surface defective ZnO nanorods with long-term stable photoelectrochemical activity.Appl. Surf. Sci.2016;383:165-76.
[28] Zheng YH, Zheng LR, Zhan YY,.Lin XY, Zheng Q, Wei KM. Ag/ZnO heterostructure nanocrystals: synthesis, characterization, and photocatalysis. Inorg. Chem.2007;46:6980-6.
[29] Park S, An J, Potts JR, Velamakanni A, Murali S, Ruoff RS. Hydrazine-reduction of graphite- and graphene oxide. Carbon.2011;49:3019.
[30] Naskar A, Bera S, Bhattacharya R, Roy SS, Jana S. Synthesis, characterization and cytotoxicity of polyethylene glycol coupled zinc oxide–chemically converted graphene nanocomposite on human OAW42 ovarian cancer cells. Polym. Adv. Technol,2016;27:436.
[31] Li B, Liu T, Wang Y, Wang Z. ZnO/graphene-oxidenanocomposite with remarkably enhanced visible-light-drivenphotocatalytic performance. J colloid interf sci.2012;377:114–21.
[32] Yang J,.Dennis R, Sardar D. Room-temperature synthesis of flowerlike Ag nanostructures consisting of single crystalline Ag nanoplates. Mater. Res. Bull.2011;46:1084.
[33] SeokKim K, Rhee KY, JinPark S. Influence of multi-walled carbon nanotubes on electrochemical performance of transparent graphene electrodes. Mater. Res. Bull.2011;46:1301-6.
[34] Murtaza G, Ahmad R, Rashid MS, Hassan M, Hussain A, Khan MA, Haq MEU, Shafique MA, Riaz S. Structural and magnetic studies on Zr doped ZnO diluted magnetic semiconductor.Curr. Appl. Phys.2014;14:176-81.
[35] Salem W, Leitner DR, Zingl FG, Schratter G, Prassl R, Goessler W, Reid J, Schild S. Antibacterial activity of silver and zinc nanoparticles against Vibrio cholerae and enterotoxic Escherichia coli. Int. J. Med. Microbiol. Suppl.2015;305:85-95.
[36] Sun L, Shao R, Tang L, Chen Z. Synthesis of ZnFe2O4/ZnO nanocomposites immobilized on graphene with enhanced photocatalytic activity under solar light irradiation. J Alloy Compd.2013;564:55-62.
[37] Sondi I, Salopek-Sondi B. Silver nanoparticles as antimicrobial agent: a case study on E. coli as a model for Gram-negative bacteria. J. Colloid Interface Sci.2004;275:177-82.
[38] Morones JR,.Elechiguerra J, Camacho A,.Ramirez JT. The bactericidal effect of silver nanoparticles.Nanotechnology.2005;16:2346. https://doi.org/10.1088/0957-4484/16/10/059.

[39] Hatchett DW, Henry S. Electrochemistry of Sulfur Adlayers on the Low-Index Faces of Silver. J. Phys. Chem.1996;100:9854–59.
[40] Liu SB, Zeng TY, Hofmann H, Burcombe M, Wei E, Jiang J,.Kong JRR, Chen Y. Antibacterial Activity of Graphite, Graphite Oxide, Graphene Oxide, and Reduced Graphene Oxide: Membrane and Oxidative Stress. ACS Nano.2011;5:6971–80.
[41] Macarno DC, Kosynkin DV, Berlin JM, Sinitskii A, Sun Z, Slesarev A, Alemany L, Lu BW, Tour JM. Improved Synthesis of Graphene Oxide. ACS Nano.2010;4:4806–14.
[42] Danilcauk M, Lund A, Saldo J, Yamada H, Michalik J, Conduction electron spin resonance of small silver particles.Spectrochim Acta A.2006;63:189-91.
[43] Akhavan O, Ghaderi E. Toxicity of Graphene and Graphene Oxide Nanowalls Against Bacteria. ACS Nano.2010;4:5731–36.
[45] Yildirim A, Mavi A, Oktay M, Kara A, Algur AO,.Bilaloglu FV. Comparison of Antioxidant and Antimicrobial Activities of Tilia (Tilia Argentea Desf Ex DC), Sage (Salvia Triloba L.), and Black Tea (Camellia Sinensis) Extracts. J. Agric. Food Chem.2000;48:5030–34.
[46] Nagmoti DM, Khatri DK, Juvekar PR, Juvekar AR. Antioxidant activity free radical-scavenging potential of Pithecellobium dulce Benth seed extracts. Free Radical and Antioxidants.2011;2:37-43.
[47] Amarowicz R, Pegg RB, Rahimi MP, Barl B. A. Weil, Free-radical scavenging capacity and antioxidant activity of selected plant species from the Canadian prairies. Food Chem. 2004;84:551-62.
[48] Shahat AS, Assar NH. Biochemical and antimicrobial studies ofbiosynthesised silver nanoparticles using aqueos extract of Myrtus communis L. Biol Res.2015;6:90-103.
[49] Panda BN, Raj AB, Shrivastava NR, Prathani AR. The evaluation of nitric oxide scavenging activity of Acalyphaindica Linn Root. Asian Journal Research Chemistry.2009;2:148–50.
[50] Motshekga CS, Raya S, Maurice S, Onyango NB, Momba M. Microwave-assisted synthesis, characterization and antibacterial activity of Ag/ZnO nanoparticles supported bentonite clay. J. Hazard. Mater.2013;262:439-446.
[51] Ankanna S, Prasad TN, Elumalai EK, Savithramma N. Production of biogenic silver nanoparticles using boswellia ovalifoliolata stem bark.Digest J.Nanomater.Biostruct.2010;5:369-72.
[52] Park J, Lim DH, Lim HJ, Kwon T, Choi JS, Jeong S. Size dependent macrophage responses and toxicological effects of Ag nanoparticles.Chem. Comm.2011;47:4382-84.
[53] Malachova K, Praus P, Rybkova Z, Kozak O. Antibacterial and antifungal activities of silver, copper and zinc montmorillonites. Appl. Clay Sci.2011;53:642-45.
[54] He D, Bligh MW, Waite TD. Effects of Aggregate Structure on the Dissolution Kinetics of Citrate-Stabilized Silver Nanoparticles. Environ. Sci. Technol.2013;47:9148- 56.
[55] Kittler S, Greulich C, Diendorf J, Koller M, Epple M. Identification Strategy Using Combined Mass Spectrometric Techniques for Elucidation of Phase I and Phase II in Vitro Metabolites of Lipophilic Marine Biotoxins. Chem. Mater.2010;22:9329-35.
[56] Li L, Sun J, Li X, Zhang Y, Wang Z,.Wang C. Controllable synthesis of monodispersed silver nanoparticles as standards for quantitative assessment of their cytotoxicity. Biomaterials.2012;33:1714-21.
[57] Trickler WJ, Lantz SM, Murdock RC, Schrand AM, Robinson BL, Newport GD. Silver Nanoparticle Induced Blood-Brain Barrier Inflammation and Increased Permeability in Primary Rat Brain Microvessel Endothelial Cells. J Toxicol Sci.2010;118:160.
[58] Cao YW, Jin R, Mirkin CA. DNA-Modified Core−Shell Ag/Au Nanoparticles. J. Am. Chem. Soc.2001;123:7961-

Figures and Tables

Table 1; Anti-inflammatory activity of Ag-RGO-ZnO composite in Mice

S. NO	Treatment of Animals	Before Formalin induced Paw Size	After formalin Induced Paw Size	Percentage of inhibition (%)			
				1h	2h	3h	4h
1.	Control	1cm	3.2cm	-	-	-	-
2.	Ag-RGO-ZnO mg/ml	1.4cm	3.2cm	6.55%	22.12%	30.5%	52.12%
3.	Standard (Paracetamol 100mg/kg)	1.6cm	3.3cm	3.43%	12.23%	21.88%	31.56%

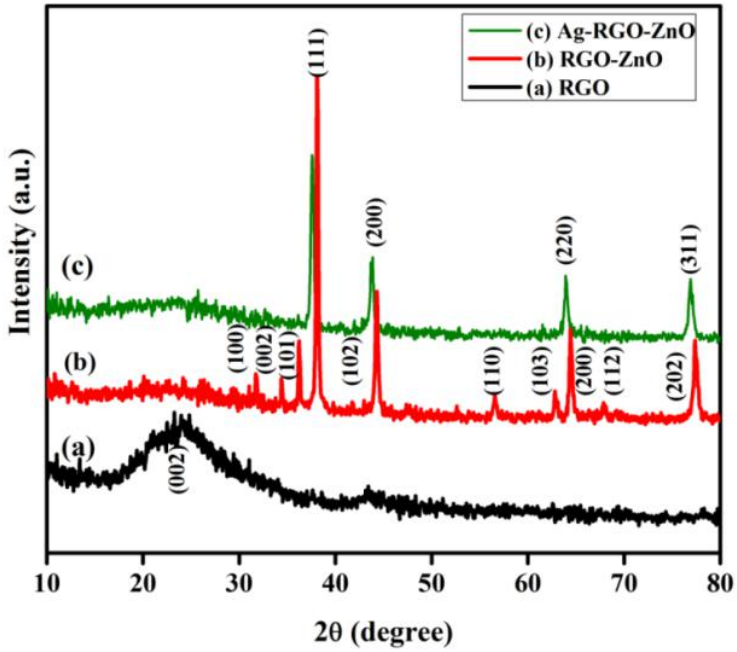

Figure.1. XRD patterns of (a) RGO, (b) RGO-ZnO, (c) Ag-RGO-ZnO hybrids.

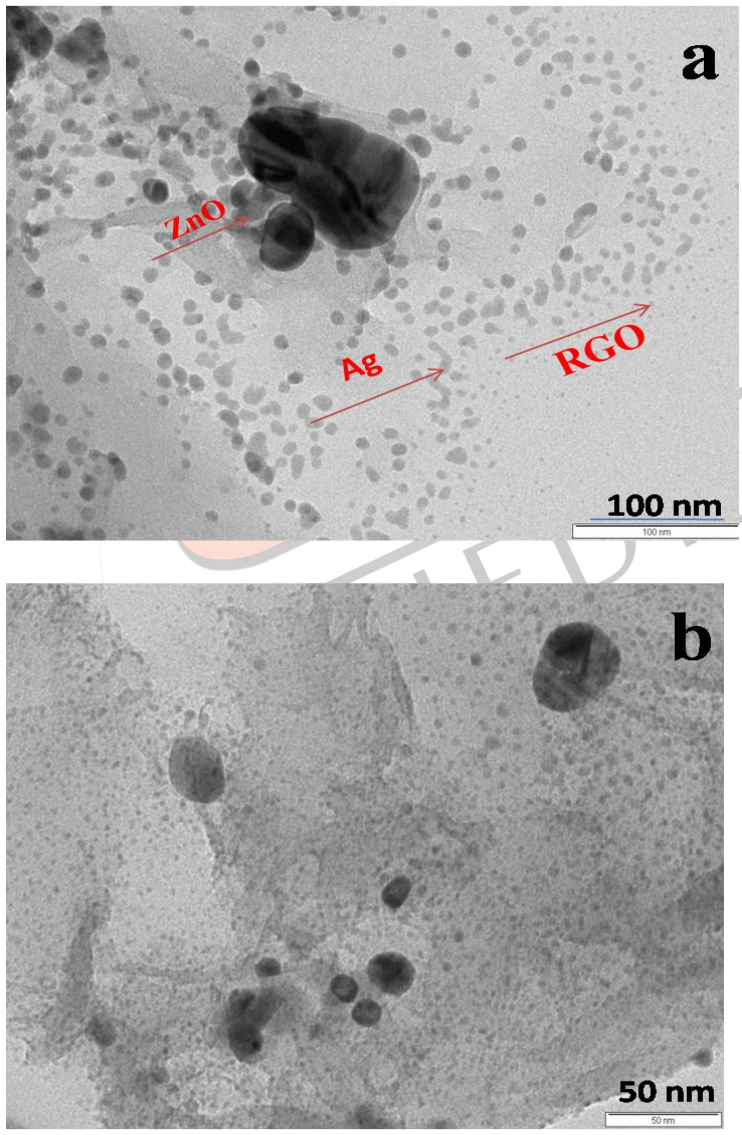

Figure.2 (a and b)HR-TEM images of RGO-ZnO hybrid at 100 and 50 nm.

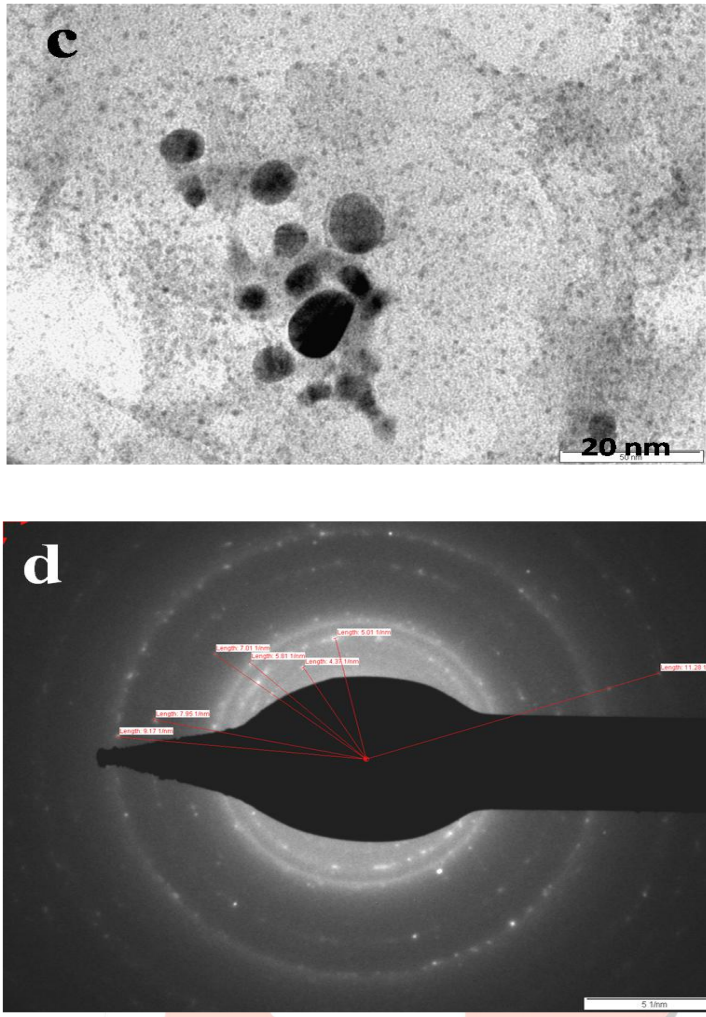

Figure.2. (c and d) HR-TEM images of RGO-ZnO hybrid with SAED pattern

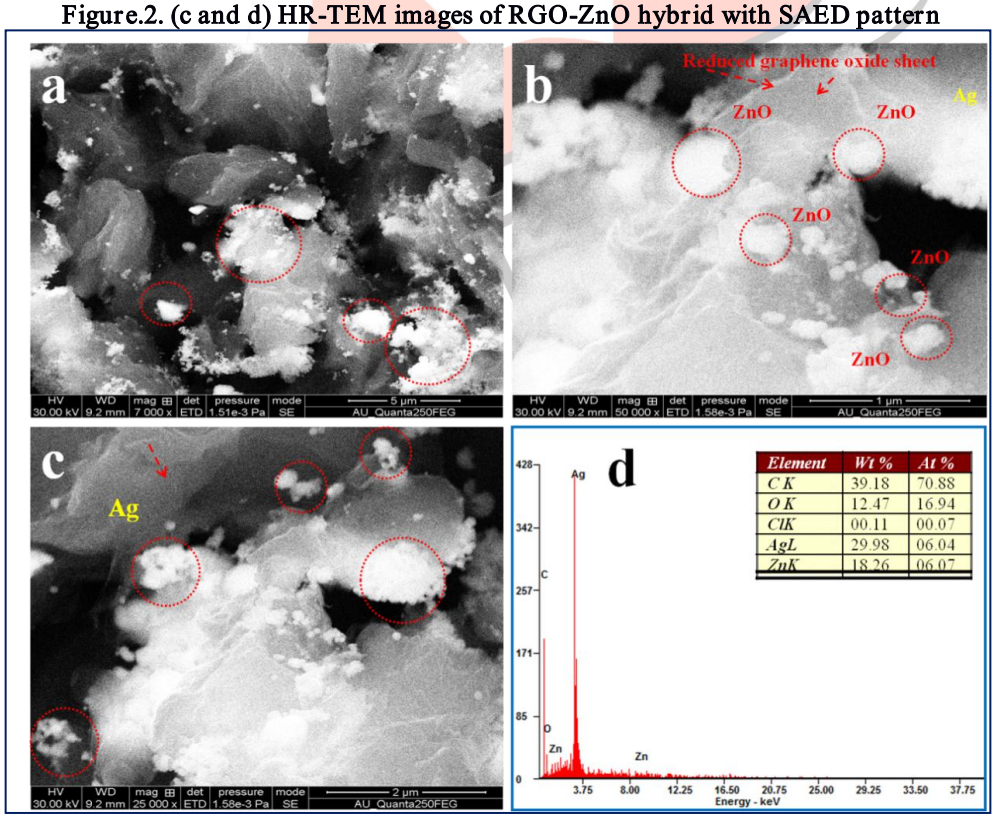

Figure.3. HR-SEM with EDX images of Ag-RGO-ZnO hybrid

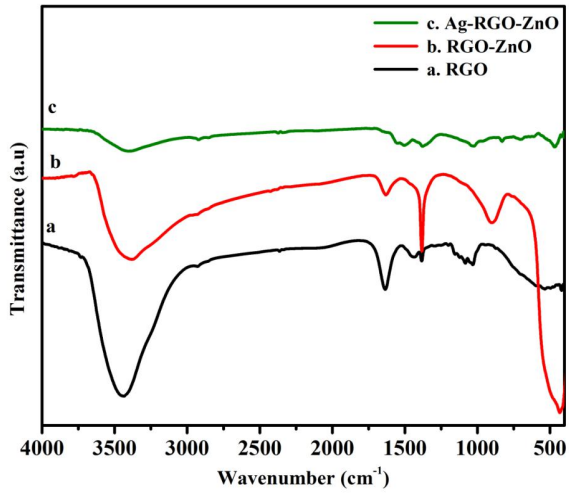

Figure.4. FT-IR spectra of Ag-RGO-ZnO hybrid.

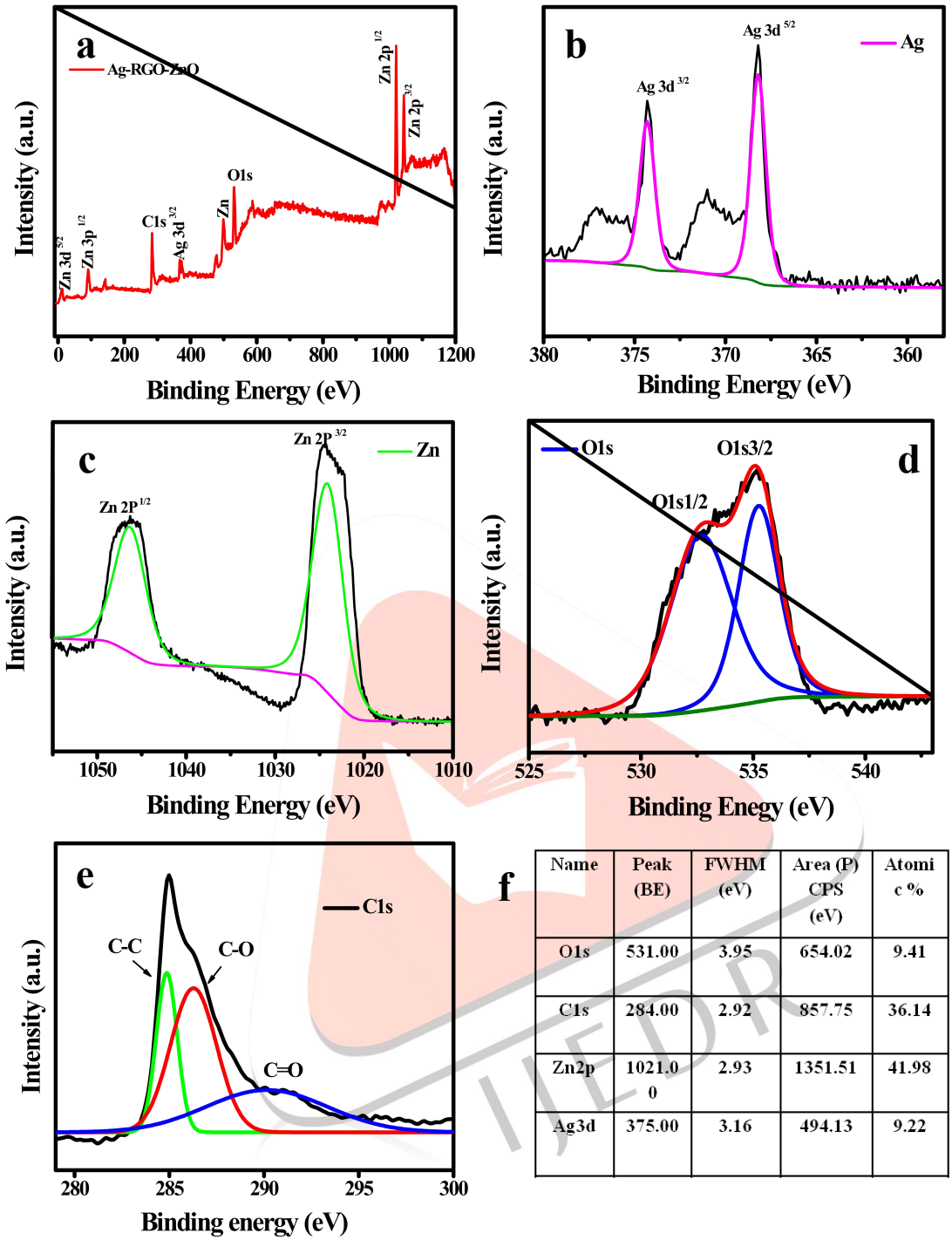

f

Name	Peak (BE)	FWHM (eV)	Area (P) CPS (eV)	Atomic %
O1s	531.00	3.95	654.02	9.41
C1s	284.00	2.92	857.75	36.14
Zn2p	1021.00	2.93	1351.51	41.98
Ag3d	375.00	3.16	494.13	9.22

Figure.5. XPS analysis of Ag-RGO-ZnO nanocomposite

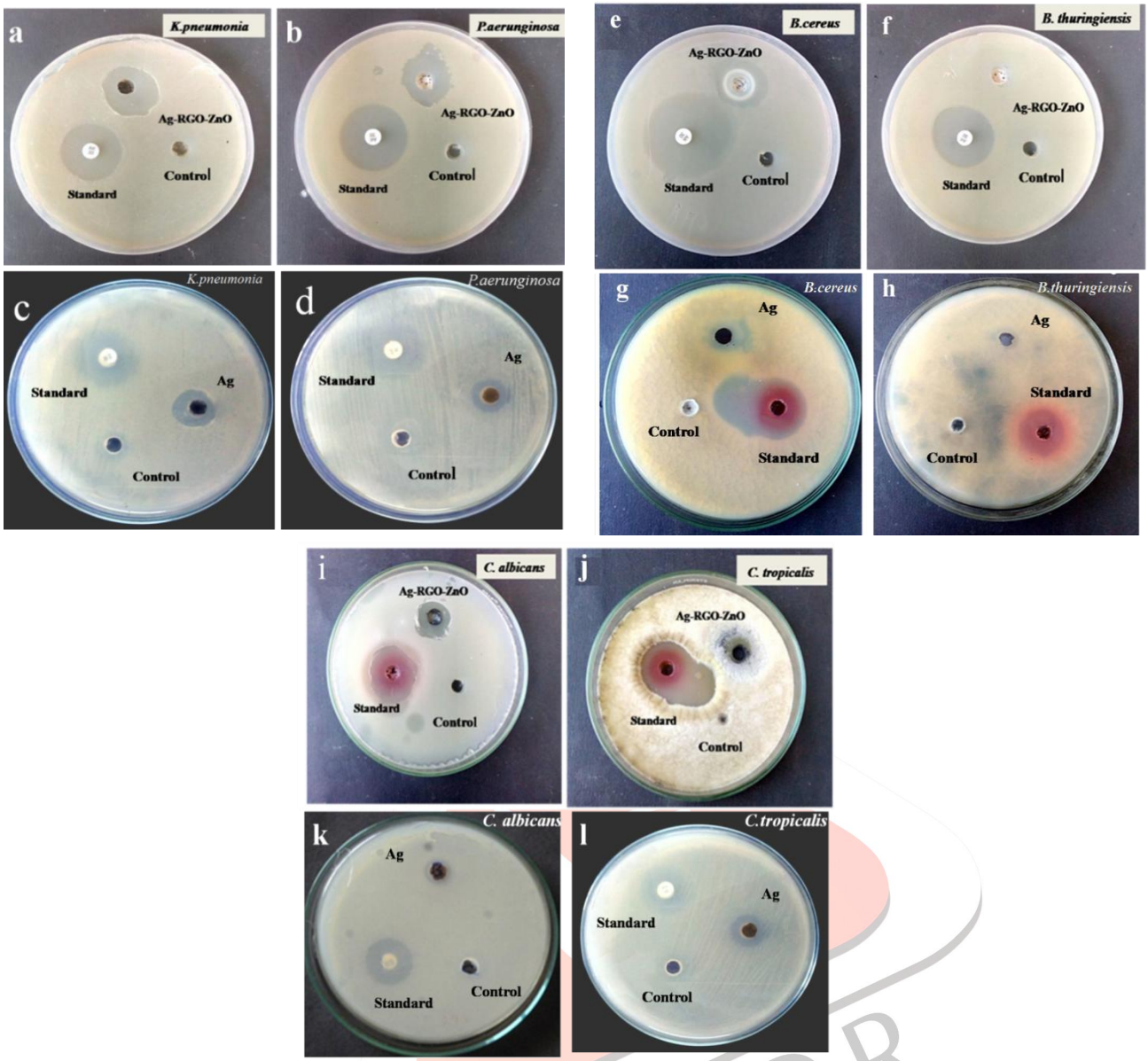

Figure.6. Antibacterial activity of Ag-RGO-ZnO hybrid (e-f) Ag (g, h) on Gram-positive bacteria with standard amikacin Figure.6. (i-l) Antifungal activity of Ag-RGO-ZnO hybrid (i, j) Ag (k, l) on fungal pathogens with standard ketoconazole

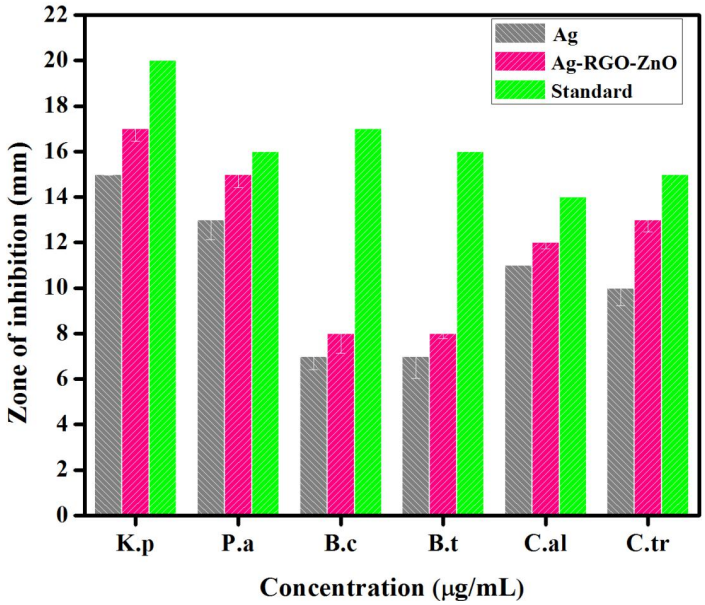

Figure.7. Antimicrobial activity histogram of Ag-RGO-ZnO hybrid

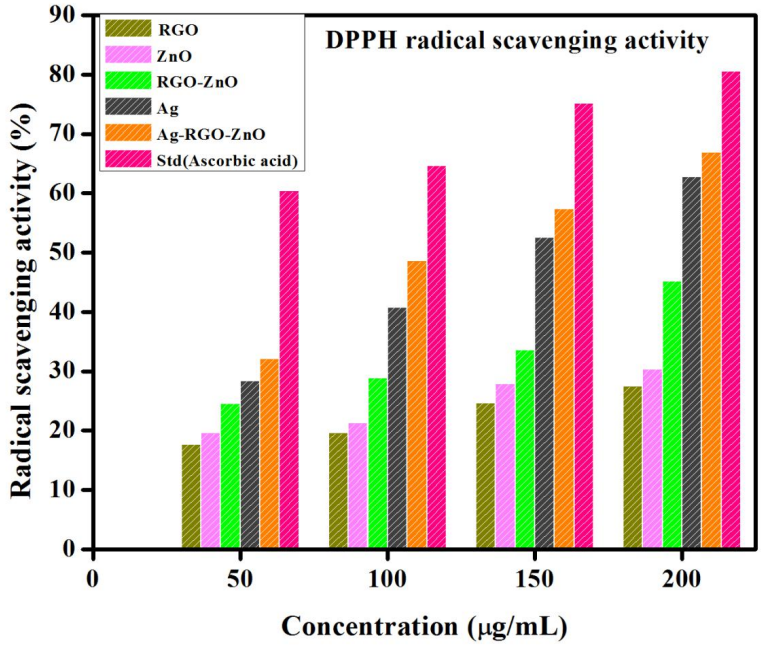

Figure. 8. DPPH radical scavenging assay of Ag-RGO-ZnO hybrid

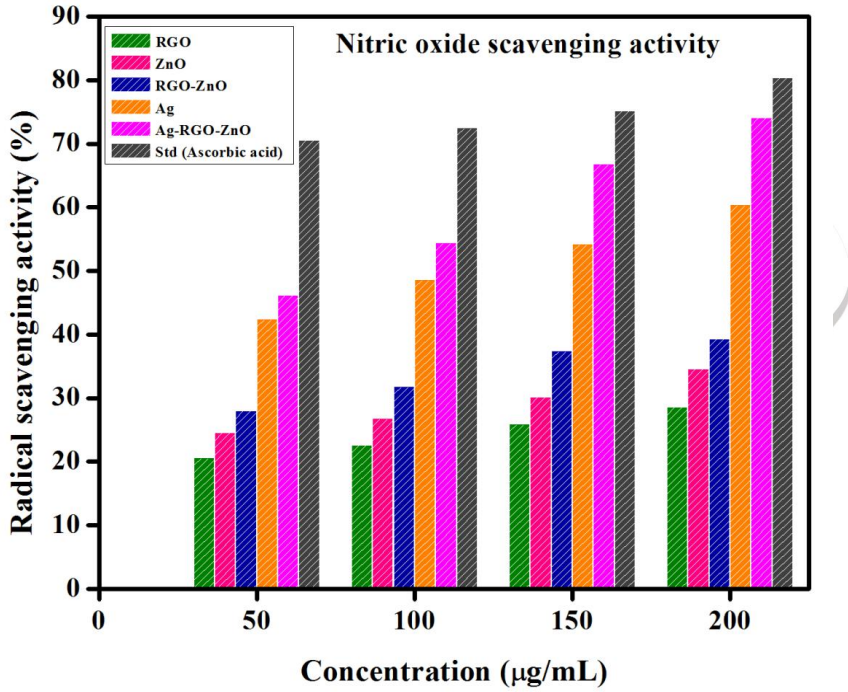

Figure. 9. Nitric oxide scavenging activity of Ag-RGO-ZnO hybrid

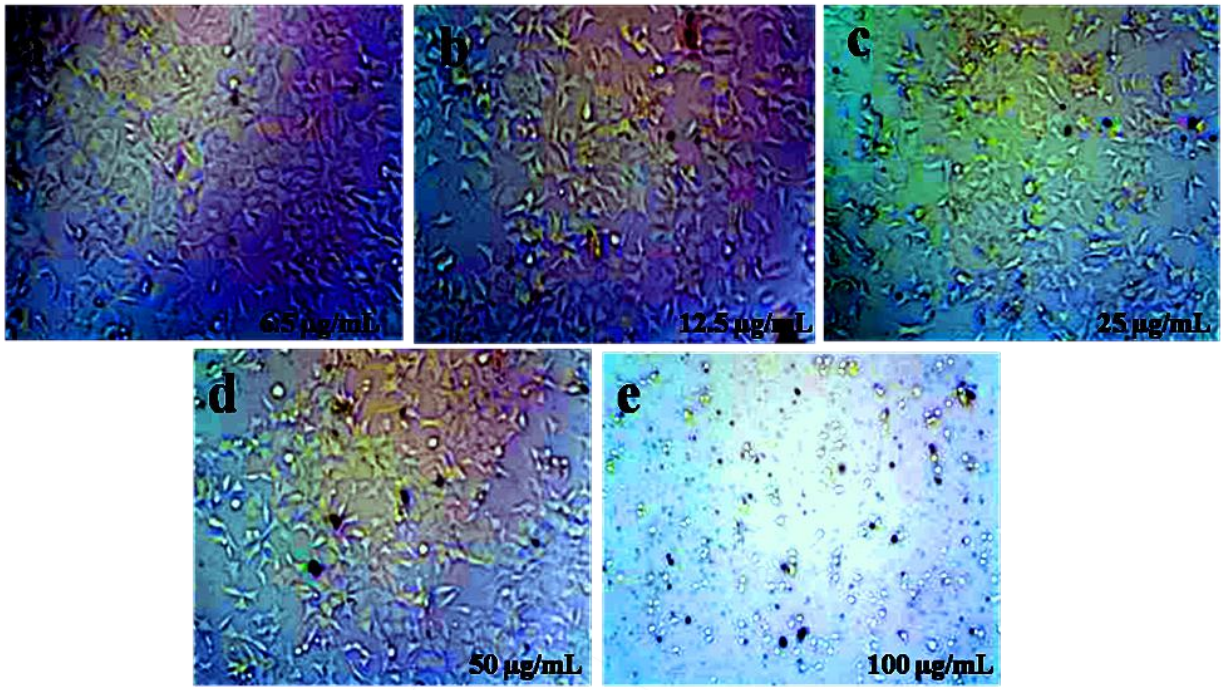

Figure.10. (a-e) Optical microscopic images of Ag-RGO-ZnO against HEK 293

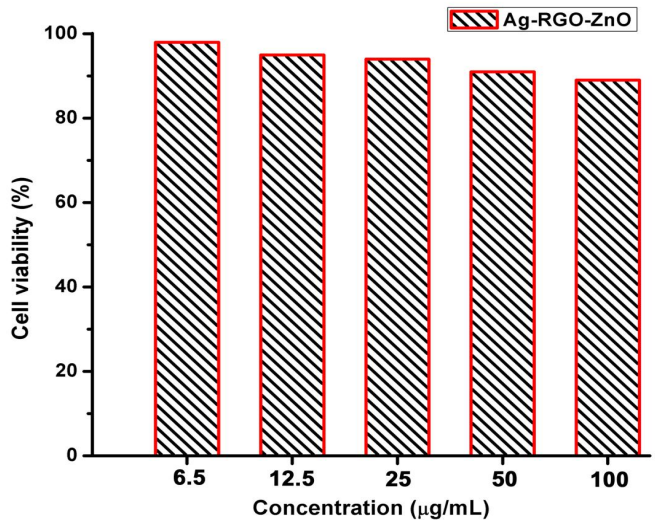

Figure.11. Cell viability histogram of Ag-RGO-ZnO against HEK 293